

## Simulation of Phase Transitions in Highly Asymmetric Fluid Mixtures

Jiwen Liu,<sup>1</sup> Nigel B. Wilding,<sup>2</sup> and Erik Luijten<sup>1</sup>

<sup>1</sup>*Department of Materials Science and Engineering, University of Illinois at Urbana-Champaign, Urbana, Illinois 61801, USA*

<sup>2</sup>*Department of Physics, University of Bath, Bath BA2 4LP, United Kingdom*

(Received 12 April 2006; published 14 September 2006)

We present a novel method for the accurate numerical determination of the phase behavior of fluid mixtures having large particle-size asymmetries. By incorporating the recently developed geometric cluster algorithm within a restricted Gibbs ensemble, we are able to probe directly the density and concentration fluctuations that drive phase transitions, but that are inaccessible to conventional simulation algorithms. We develop a finite-size scaling theory that relates these density fluctuations to those of the grand-canonical ensemble, thereby enabling accurate location of critical points and coexistence curves of multicomponent fluids. Several illustrative examples are presented.

DOI: [10.1103/PhysRevLett.97.115705](https://doi.org/10.1103/PhysRevLett.97.115705)

PACS numbers: 64.70.Fx, 05.10.Ln, 64.70.Ja, 82.70.Dd

The vast majority of commercially relevant fluids are multicomponent mixtures. An understanding of the phase behavior of these systems is of paramount importance for applications, and also a matter of great fundamental interest [1]. With the advent of powerful computers, various computational techniques have been devised to directly determine fluid phase behavior [2]. However, these methods are all restricted to fluids in which the various components have similar sizes, whereas important phenomena occur in highly size-asymmetric multicomponent fluids such as colloidal dispersions, colloid-nanoparticle mixtures, and polymer solutions [1,3].

The computational bottleneck for existing simulation methods arises from the fact that they cannot simultaneously relax a fluid system on disparate length scales. Specifically, for large size ratios, the big particles become “jammed” by the smaller ones. Recently, however, building on earlier work [4], a geometric cluster Monte Carlo algorithm (GCA) was proposed [5,6] that facilitates *rejection-free* simulations of highly size-asymmetric mixtures via large-scale collective updates which move whole groups of particles in a single step. Although this method has been successfully applied to problems relating to colloidal stabilization [7,8], in which size asymmetries span several orders of magnitude, it is incapable of dealing with the density and concentration fluctuations associated with phase separation, since it inherently operates in a canonical ensemble in which the particle number and volume are fixed. This limitation cannot be overcome by incorporating cluster moves into a standard grand-canonical (GC) or constant- $NpT$  ensemble, because this does not address the underlying shortcomings of these ensembles with respect to sampling of density fluctuations in asymmetric mixtures.

It is the purpose of this Letter to introduce a method that overcomes these problems. This is achieved by embedding cluster moves in a variant of the Gibbs ensemble [9,10], in such a way that they *couple* to the density fluctuations, resulting in efficient exploration of configuration space. To

exploit this approach we present a finite-size scaling theory that permits the determination of the critical point and the phase boundary. As an illustration, we apply the method to study liquid-vapor coexistence in asymmetric binary mixtures, for which we show that the presence of even small quantities of small-particle additives can strongly affect the location of the critical point. Furthermore, depending on the nature of the interaction of the additive with the fluid particles, the critical temperature can either be enhanced or depressed.

To enable density fluctuations, we distribute a prescribed number of particles  $N_0$  over two boxes, and devise an operation that exchanges particles between these boxes [9] to maintain chemical equilibrium. By adopting the symmetrical *restricted* Gibbs (RG) ensemble [10], in which the boxes have equal *constant* volumes  $V = L^d$ , geometric cluster moves can be used for this exchange operation. The prescription for a cluster move closely follows the original algorithm [5], with the crucial difference that a geometric operation not only alters the position of a particle, but also transfers it from one box to the other. Specifically, a pivot is placed at a random position within the first box, as well as at the corresponding position within the second box. A particle  $i$  is picked at random from one of the boxes (denoted 1) and point-reflected with respect to the pivot from its original position  $\mathbf{r}_i$  to  $\mathbf{r}'_i$ . However, instead of placing the particle at  $\mathbf{r}'_i$ , we place it at the corresponding point  $\bar{\mathbf{r}}'_i$  in the other box (denoted 2), subject to periodic boundary conditions. Thereafter, any particle  $j$  interacting with particle  $i$  around its original position in box 1 or its new position in box 2 will also be considered for point reflection around the pivot and subsequent transfer to the opposite box, with a probability  $p_{ij} = \max[1 - \exp(-\beta\Delta_{ij}), 0]$ , where  $\Delta_{ij} = -V(|\mathbf{r}_i - \mathbf{r}_j|)$  if particles  $i$  and  $j$  originally reside in the same box and  $\Delta_{ij} = V(|\bar{\mathbf{r}}'_i - \mathbf{r}_j|)$  if  $i$  and  $j$  originally reside in different boxes.  $V(r)$  denotes a general pair potential and  $\beta$  the inverse temperature  $1/k_B T$ . Note that  $p_{ij}$  *solely* depends on the pair

interaction between particles  $i$  and  $j$ , rather than on the total energy change resulting from the displacement of particle  $j$ . The cluster construction proceeds iteratively for all particles interacting with each particle  $j$ . Upon completion of a cluster move, a new pivot is selected. The proof of detailed balance is analogous to that for the generalized GCA [5,6].

The exchange of particles between boxes leads to (complementary) density fluctuations around the average number density  $\rho_0 = N_0/(2V)$  in each box. The fluctuation spectrum of the number density in box 1,  $\rho_1 = N_1/V$ , can be related to the *grand-canonical* probability distributions  $P$  of the number densities of both boxes via [11]

$$P^{\text{RG}}(\rho_1|\rho_0, V, T) \propto P(\rho_1|\mu, V, T)P(2\rho_0 - \rho_1|\mu, V, T), \quad (1)$$

where we note that  $P^{\text{RG}}(\rho_1)$  is independent of the choice of chemical potential  $\mu$  on the right-hand side [11].  $P^{\text{RG}}(\rho_1)$  is symmetric (even) with respect to its mean  $\bar{\rho}_1 = \rho_0$ . To facilitate comparison of the forms of  $P^{\text{RG}}(\rho_1)$  for various choices of  $\rho_0$ , it is expedient to consider distributions of zero mean, to which end we define  $x = \rho_1 - \rho_0$  and write

$$P^{\text{RG}}(x|\rho_0, T) \propto P(x + \rho_0|T)P(-x + \rho_0|T), \quad (2)$$

where we have suppressed reference to the constant volume  $V$  and the (arbitrary) chemical potential  $\mu$ .

The parameter space of the RG ensemble is spanned by  $\rho_0$  and  $T$ . In the vicinity of the critical point  $(\rho_0^c, T^c)$  terminating a line of liquid-vapor coexistence of a pure fluid or fluid mixture,  $P^{\text{RG}}$  exhibits universal scaling behavior. Introducing reduced variables  $\varrho_0 \equiv (\rho_0 - \rho_0^c)/\rho_0^c$  and  $t \equiv (T - T^c)/T^c$ , we make the following ansatz for the finite-size scaling (FSS) properties of  $P^{\text{RG}}(x)$ ,

$$P_L^{\text{RG}}(x|\varrho_0, t) = a_0 L^{\beta/\nu} \tilde{P}^{\text{RG}}(a_0 L^{\beta/\nu} x, a_1 \varrho_0 L^{\beta/\nu}, a_2 t L^{1/\nu}). \quad (3)$$

Here  $\tilde{P}^{\text{RG}}$  is a universal function which is *symmetric* in  $x$  for all values of  $t$  and  $\varrho_0$ ;  $\beta$  and  $\nu$  are critical exponents, and  $a_0, a_1, a_2$  are nonuniversal metric factors. The arguments in  $t$  and  $\varrho_0$  control deviations from criticality. The temperature field has the form familiar from the FSS properties of magnets [12] or fluids [13], while that in  $\varrho_0$  is particular to the RG ensemble. As one can verify [14] from an expansion of Eq. (2) with respect to  $\rho_0$ , together with the known [13] symmetry properties of the derivatives of  $P(x)$ , variations in the form of  $P^{\text{RG}}(x)$  are—to leading order—controlled by the value of  $\rho_0^2$ ; all terms having odd powers of  $\rho_0$  are antisymmetric in  $x$  and hence absent on symmetry grounds.

To characterize the form of  $\tilde{P}^{\text{RG}}(x)$  as a function of  $\varrho_0$  and  $t$ , it is useful to consider the behavior of the dimensionless fourth-order cumulant ratio  $Q \equiv \langle x^2 \rangle^2 / \langle x^4 \rangle$  [12], whose scaling properties follow from Eq. (3) as

$$Q_L(\varrho_0, t) = \tilde{Q}(q_1 \varrho_0 L^{\beta/\nu}, q_2 t L^{1/\nu}), \quad (4)$$

with  $\tilde{Q}$  a universal function and  $\tilde{Q}(0, 0) \equiv Q^*$ . The value of  $Q^* = 0.711901$  is known *a priori* by virtue of the result that  $\tilde{P}^{\text{RG}}(a_0 L^{\beta/\nu} x, 0, 0) \propto [P^*(L^{\beta/\nu} m)]^2$  [11], with  $P^*(L^{\beta/\nu} m)$  the universal critical Ising magnetization distribution [15]. Measurements of  $Q_L(\varrho_0, t)$  for a range of global densities  $\rho_0$  provide a useful route to locating criticality. Specifically, consider the locus of points in  $\varrho_0$ - $t$  space for which  $Q_L(\varrho_0, t) = Q^*$ , which we term the “iso- $Q^*$  curve.” Expanding Eq. (4) with respect to  $t < 0$  and  $\varrho_0$ , and recalling that only terms involving even powers of  $\varrho_0$  are nonzero, one has

$$Q_L(\varrho_0, t) = Q^*[1 + q_1 \varrho_0^2 L^{2\beta/\nu} + q_2 t L^{1/\nu} + \mathcal{O}(\varrho_0^4, t^2)], \quad (5)$$

from which it follows that, sufficiently close to the critical point, the iso- $Q^*$  curve is a *parabola* in  $\varrho_0$ - $t$  space,

$$\varrho_0^2 = -(q_2/q_1)L^{(1-2\beta)/\nu}t. \quad (6)$$

The maximum of this parabola (at  $\varrho_0 = t = 0$ ) coincides with the critical point and hence, by fitting to a few estimated points on the iso- $Q^*$  curve, one can readily determine the critical parameters  $\rho_0^c$  and  $T^c$ .

Turning now to the task of obtaining subcritical coexistence properties within the RG framework, we consider the peak positions of  $P^{\text{RG}}(\rho_1|\rho_0, t)$  on an isotherm. When  $\rho_0$  equals the coexistence diameter  $\rho_d \equiv (\rho_g + \rho_l)/2$ , with  $\rho_g$  and  $\rho_l$  the gas and liquid densities, the peak positions of  $P^{\text{RG}}(\rho_1)$  coincide with the coexisting densities, which can thus be read off from a histogram of its form [16]. An effective method for locating  $\rho_d$  exploits the fact that the even moments of  $P^{\text{RG}}(x|\rho_0, t)$  are maximized when  $\rho_0 = \rho_d$ . From the absence of odd powers of  $\rho_0$  in the expansion of Eq. (2), it can then be shown [14] that the variance  $\sigma^2(\rho_0|t)$  of  $P^{\text{RG}}(x|\rho_0, t)$  varies to leading order quadratically in  $(\rho_0 - \rho_d)$ , i.e.,

$$\sigma^2(\rho_0|t) = \sigma^2(\rho_d, t) - b(\rho_0 - \rho_d)^2, \quad (7)$$

with  $b$  a positive constant. By fitting to estimates of  $\sigma^2(\rho_0|t)$ , this result facilitates a determination of  $\rho_d$  and thence the coexisting densities.

To test the scaling theory, we first perform simulations using the GCA in the restricted Gibbs ensemble for a pure Lennard-Jones (LJ) fluid. We employ a potential cutoff  $2.5\sigma$  and reduced system sizes  $L^* = L/\sigma = 10, 20, 30$ . At fixed global density  $\rho_0$ , histogram reweighting can be used to determine a point on the iso- $Q^*$  curve, i.e., the temperature at which  $Q_L(\rho_0, T)$  takes the value  $Q^*$ . Repeating for a range of  $\rho_0$  values allows the entire iso- $Q^*$  line to be mapped. As shown in Fig. 1, the iso- $Q^*$  curves for the various  $L^*$  are indeed parabolas [cf. Eq. (6)] that coincide at their maximum. A careful analysis [14] of the position of this maximum,  $\tilde{T}^c = k_B T^c / \varepsilon = 1.1878(2)$ ,  $\tilde{\rho}^c = \rho_0^c \sigma^3 = 0.3204(5)$ , reveals excellent agreement with an existing GC estimate,  $\tilde{T}^c = 1.1876(3)$ ,  $\tilde{\rho}^c = 0.3197(4)$

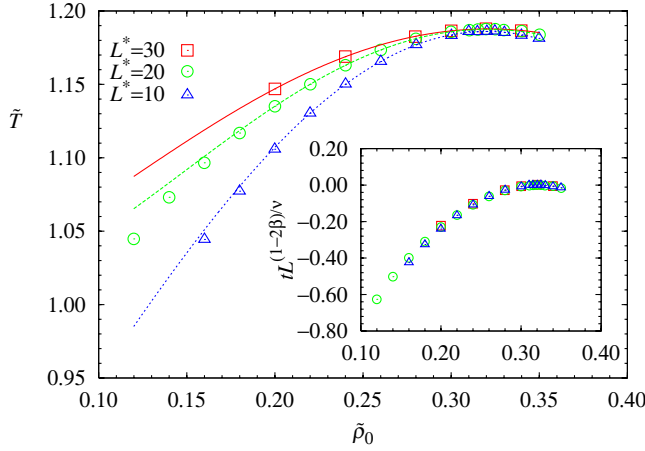


FIG. 1 (color online). Measured iso- $Q^*$  points (symbols) for pure LJ fluid, together with parabolic fits (curves). The maxima of the curves (shown for  $L/\sigma = 10, 20, 30$ ) in the  $\tilde{\rho}_0$ - $\tilde{T}$  plane correspond to the critical point. The data collapse in the inset confirms the scaling prediction [Eq. (6)].

[17]. The inset confirms the finite-size scaling predicted in Eq. (6) with remarkable accuracy. Furthermore, the critical density distribution  $\tilde{P}^{\text{RG}}(x)$  is indeed in quantitative agreement (not shown) with the square of the critical Ising magnetization distribution, as predicted [11].

Having established the validity of our methodology, we exploit the GCA to address a typical problem that is intractable for conventional simulations. We consider a binary, strongly size-asymmetric mixture of LJ particles of size  $\sigma$  and small particles (“additives”) of diameter  $\sigma_s = \sigma/10$ . Depending on their interaction with the large particles, the presence of additives will affect the phase behavior and shift the location of the liquid-vapor critical point compared to the pure fluid. The additives mutually interact via a weakened LJ potential,

$$V_{ss}(r) = 4\left(\frac{\varepsilon}{10}\right)\left[\left(\frac{\sigma_s}{r}\right)^{12} - \left(\frac{\sigma_s}{r}\right)^6\right] \quad (r < 2.5\sigma_s), \quad (8)$$

whereas a large and a small particle interact as hard spheres at a separation  $\sigma_{ls} = (\sigma + \sigma_s)/2$ .

As before, we perform simulations for a range of  $\rho_0$ , at fixed additive volume fraction  $\phi_s = \frac{\pi}{6}\sigma_s^3\rho_s = 0.005$ , corresponding to  $N_s = 10000$ . Because the small particles are so numerous, and disperse relatively homogeneously, the insertion probability of a large particle in a standard GC approach would be prohibitively small. By contrast, the present scheme renders it feasible to equilibrate the system and sample the density fluctuations. Figure 2 (diamonds) shows that the iso- $Q^*$  curve (plotted as a function of the total reduced density  $\tilde{\rho}_0 \equiv \rho_l\sigma^3 + \rho_s\sigma_s^3$ ) again has a parabolic shape. However, despite the small volume fraction of additives, the maximum of this curve, i.e., the liquid-vapor critical point of the mixture, is markedly shifted. The increase in the critical temperature reflects an enhanced attraction between the large particles which

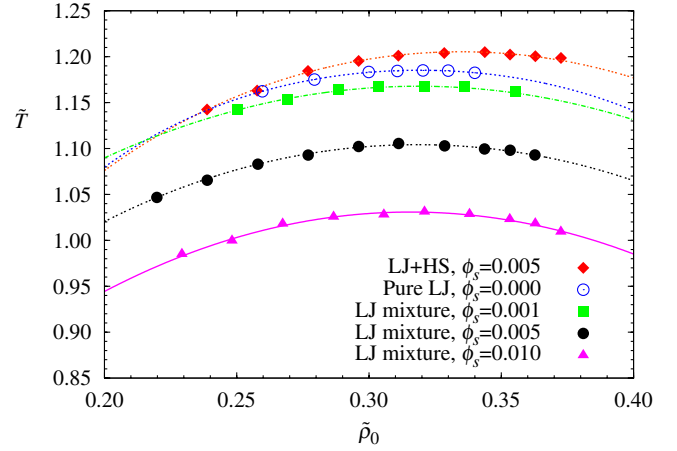


FIG. 2 (color online). Iso- $Q^*$  curves for size-asymmetric binary mixtures consisting of a LJ fluid (particle size  $\sigma$ ) and small additives (particle diameter  $\sigma/10$ , volume fraction  $\phi_s$ ). All curves pertain to a linear system size  $L = 8.06\sigma$ . For additives that interact with the fluid as hard spheres (diamonds, upper curve), the critical temperature and density increase compared to the pure fluid (open circles), whereas the critical temperature decreases strongly if the additives have a weak attraction with the fluid (squares, filled circles, triangles).

stems from the entropic depletion interactions induced by the additives [18].

To highlight the subtle role of the *interactions* of the additives with the larger species we study a system in which there is a weak attraction between large and small particles. The interaction is again of the LJ form, Eq. (8), in which  $\sigma_s$  is replaced with  $\sigma_{ls}$ . Already at  $\phi_s = 10^{-3}$  the critical temperature is now noticeably *depressed*, as is evident from the shift of the iso- $Q^*$  maximum in Fig. 2, and at  $\phi_s = 10^{-2}$ ,  $T^c$  has decreased by almost 20%. We explain this surprising effect by the formation of a shell of small particles around the large particles, akin to nanoparticle halo formation [3,7,8], which weakens the effective attraction between the large particles.

Our approach not only yields accurate estimates of critical points, but also entire coexistence curves. As described above, for each subcritical temperature, the variance of  $P^{\text{RG}}(x)$  has a maximum at the coexistence curve diameter  $\rho_d$  [Eq. (7)], as is confirmed in Fig. 3. The (total) densities of the coexisting liquid and vapor phases are determined from the peak positions of  $P^{\text{RG}}$  [cf. Fig. 4(a)], resulting in the phase diagram in Fig. 4(b). We emphasize that obtaining such a phase diagram in a reasonable time scale would not be feasible using even the most efficient traditional approach to fluid phase equilibria, namely, GC simulation [17]. Our tests show that the GC relaxation time is too large to be reliably estimated. Nevertheless, a lower bound on the GC relaxation time can be estimated via a comparison of the large-particle transfer (insertion or deletion) acceptance probability  $p_{\text{acc}}$ . For liquidlike densities of the large particles ( $\tilde{\rho}_1 \approx 0.6$ ),

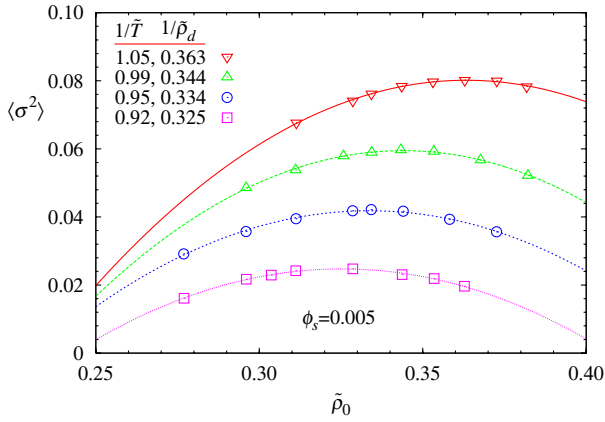


FIG. 3 (color online). Variance of  $P^{\text{RG}}(x)$  for a LJ mixture with size asymmetry  $\sigma/\sigma_s = 10$ , as a function of total number density  $\tilde{\rho}_0$ . Each (isothermal) curve is obtained from simulations at selected densities, but with constant additive volume fraction  $\phi_s = 0.005$ , and is parabolic (see fits), confirming Eq. (7). The maxima locate the coexistence curve diameter.

we find that for  $\phi_s = 0.005$ ,  $p_{\text{acc}} \sim 10^{-4}$ ; while for  $\phi_s = 0.01$ , this falls to  $p_{\text{acc}} \sim 10^{-6}$ . These values are to be compared with  $p_{\text{acc}} \sim 10^{-1}$  for the pure LJ fluid. One can therefore expect the GC relaxation time of the mixtures we have studied to be several orders of magnitude greater than for the pure LJ fluid. Since the algorithm presented here operates along fundamentally distinct lines—large-scale collective updates of clusters of small and large particles are accepted with *unit* probability—it is not hampered by this problem. Consequently, it allows the efficient calculation of phase diagrams, even under conditions for which the GC approach fails.

Summarizing, we have extended the rejection-free GCA to the study of phase transitions, by embedding it within a restricted Gibbs ensemble. The accurate location of critical points and coexistence curves within this ensemble requires a suitable FSS theory, which has been presented as well. We have applied our method to a strongly size-asymmetric LJ mixture, which cannot be studied with existing direct methods. We find that the liquid-vapor phase behavior is highly sensitive to the concentration of small particles and the nature of their interaction with the large ones. Thus our method should prove useful in predicting the alterations to phase behavior which occur when small particles of various types are added to a fluid. Furthermore, by employing the method with a variant of the GCA suitable for electrostatic interactions [19], it becomes possible to study the effects of adding salt on the phase behavior of charged colloids. Finally, we note that while for concreteness we have developed the formalism for the case of phase transitions whose order parameter is the density, the structure of our theory holds also for con-

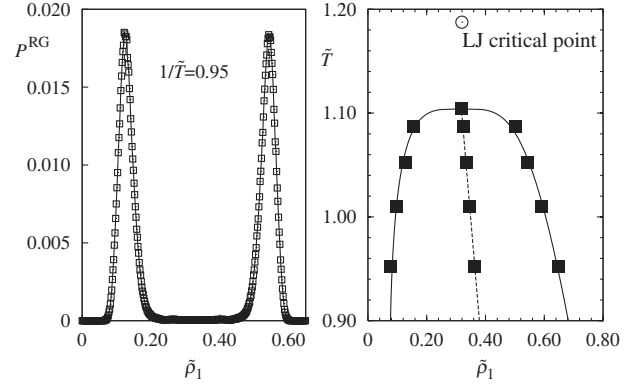


FIG. 4. (a) Example of a  $P^{\text{RG}}$  at  $\rho_0 = \rho_d$ , for the fluid mixture described in Fig. 3. (b) Corresponding phase diagram; the open circle indicates the critical point of a pure LJ fluid. The full line is a fit of the form  $\rho^\pm - \rho^c = ut + vt^\beta$ .

solute points, or indeed situations where the order parameter is a linear combination of density and concentration.

This material is based upon work supported by the National Science Foundation under Grant No. DMR-0346914 (to E. L.) and by EPSRC Grant No. GR/S59208/01 (to N. B. W.).

- [1] R. G. Larson, *The Structure and Rheology of Complex Fluids* (Oxford University, Oxford, 1999).
- [2] D. Frenkel and B. Smit, *Understanding Molecular Simulation* (Academic, San Diego, 2002), 2nd ed.
- [3] V. Tohver *et al.*, Proc. Natl. Acad. Sci. U.S.A. **98**, 8950 (2001).
- [4] C. Dress and W. Krauth, J. Phys. A **28**, L597 (1995).
- [5] J. Liu and E. Luijten, Phys. Rev. Lett. **92**, 035504 (2004).
- [6] J. Liu and E. Luijten, Phys. Rev. E **71**, 066701 (2005).
- [7] J. Liu and E. Luijten, Phys. Rev. Lett. **93**, 247802 (2004).
- [8] C. J. Martinez *et al.*, Langmuir **21**, 9978 (2005).
- [9] A. Z. Panagiotopoulos, Mol. Phys. **61**, 813 (1987).
- [10] K. K. Mon and K. Binder, J. Chem. Phys. **96**, 6989 (1992).
- [11] A. D. Bruce, Phys. Rev. E **55**, 2315 (1997).
- [12] K. Binder, Z. Phys. B **43**, 119 (1981).
- [13] A. D. Bruce and N. B. Wilding, Phys. Rev. Lett. **68**, 193 (1992).
- [14] J. Liu, N. B. Wilding, and E. Luijten (to be published).
- [15] M. M. Tsypin and H. W. J. Blöte, Phys. Rev. E **62**, 73 (2000).
- [16] This is confirmed by inserting  $\rho_0 = (\rho_g + \rho_l)/2$  into Eq. (1); clearly when  $\rho_1 = \rho_g$ , one has  $2\rho_0 - \rho_g = \rho_l$  and thus both  $P(\rho_1|t)$  and  $P(2\rho_0 - \rho_1|t)$  are maximized, implying that so too is  $P^{\text{RG}}(\rho_1)$ . The same holds for  $\rho_1 = \rho_l$ .
- [17] N. B. Wilding, Phys. Rev. E **52**, 602 (1995).
- [18] S. Asakura and F. Oosawa, J. Chem. Phys. **22**, 1255 (1954).
- [19] S. A. Barr and E. Luijten (to be published).